Use of HAND terrain descriptor for estimating flood-prone areas in river basins

Uso do descritor de terreno HAND na estimativa de áreas suscetíveis a inundações em bacias hidrográficas

Ana Alice Rodrigues Dantas[1] , Adriano Rolim Paz[1]

ABSTRACT

The flood hazard mapping in a river basin is crucial for flooding risk management, mitigation strategies, and flood forecasting and warning systems, among other benefits. One approach for this mapping is based on the HAND (Height Above Nearest Drainage) terrain descriptor, directly derived from the Digital Elevation Model (DEM), in which each pixel represents the elevation difference of this point in relation to the river drainage network to which it is connected. Considering the Mamanguape river basin (3,522.7 km²; state of Paraíba, Brazil) as the study location, the present research applied this method and verified it as for five aspects: consideration of a spatially variable minimum drainage area for denoting the river drainage initiation; the impact of considering a depressionless DEM; evaluation of hydrostatic condition; effect of incorporating an existing river vector network; and comparative analysis of basin morphology regarding longitudinal river profiles. According to the results, adopting a uniform minimum drainage area for the river network initiation is a simplification that should be avoided, using a spatially variable approach, which influences the amount and spatial distribution of flooded areas. Additionally, considering the depressionless DEM leads to higher values of HAND and to a smaller flooded area (difference ranging between 3% and 99%), when compared with the use of DEM with depression, despite 3.1% of the pixels representing depressions. The use of the depressionless DEM is recommended, whereas the DEM pre-processing by incorporating a vector network (stream burning) generates dubious results regarding the relation between HAND and the morphological pattern presented in the DEM. Moreover, the estimation of flooded areas based on HAND does not guarantee the hydrostatic condition, but this disagreement comprises a negligible area for practical purposes.

Keywords: geomatics; digital elevation model; floods.

RESUMO

O mapeamento de áreas inundáveis em uma bacia hidrográfica é fundamental para o gerenciamento do risco de inundações, estratégias mitigadoras e sistemas de previsão e alerta, entre outros benefícios. Uma abordagem para esse mapeamento é com base no descritor do terreno HAND (*Height Above Nearest Drainage*), derivado diretamente do Modelo Digital de Elevação (MDE), no qual cada pixel apresenta a diferença de elevação desse ponto em relação ao ponto da rede de drenagem ao qual ele se conecta. Considerando a bacia do rio Mamanguape (3.522,7 km²; Paraíba) como área de estudo, esta pesquisa adotou esse método e verificou sua aplicabilidade quanto a cinco aspectos: consideração de uma área mínima variável espacialmente para denotar o início da drenagem; impacto de considerar o MDE sem depressões; avaliação da condição hidrostática; efeito de incorporação de uma rede vetorial existente; análise comparativa à morfologia da bacia em termos do perfil longitudinal dos rios. Os resultados indicaram que adotar um valor uniforme de área mínima de contribuição para início da rede de drenagem é uma simplificação que deveria ser evitada, adotando-se a variação espacial de tal parâmetro, que influi no total e na distribuição espacial das áreas inundadas. Além disso, considerar o MDE sem depressões leva a maiores valores do HAND e menor área inundada (diferença variou de 3% a 99%), comparativamente ao MDE com depressões, embora apenas 3,1% dos pixels representem depressões. É recomendado considerar o MDE sem depressões, ao passo que o pré-processamento por incorporação de rede vetorial (*stream burning*) gera resultados incoerentes quanto à relação do HAND com o padrão morfológico representado no MDE. Concluiu-se, ainda, que a estimativa de áreas inundáveis pelo HAND não garante a condição hidrostática, mas esse desacordo abrange uma região de extensão desprezível para fins práticos.

Palavras-chave: geomática; modelo digital de elevação; cheias.

Introduction

Flood is a natural process that has occurred worldwide, even before human existence itself, and has been a decisive factor in the rise and development of civilizations and the decadence of others (Goerl et al., 2017). Flood events result from multiple and dynamic factors such as intense rainfall, low soil infiltration capacity or changes in land cover and land use patterns (Ali et al., 2020). This has motivated several studies to be carried out such as on the trend of occurrence of extreme events (Lira and Cardoso, 2018; Paprotny et al., 2018), the resilience to these events (Fernandes and Valverde, 2017; Heinzlef et al., 2020), and concerning climate change projections related to flood risk (Alfieri et al., 2017; Bork et al., 2017).

The association of urbanization with the intense soil impermeabilization and the reduction of vegetation cover, in addition to river drainage network modifications, leads to runoff increase, infiltration reduction, and a consequent decrease in groundwater recharge (Benini and Mendiondo, 2015). These aspects, associated with the greater occupation of high vulnerability areas, intensify the occurrence of disasters, such as floods (Speckhann et al., 2018), with a higher number of victims and higher damage costs of different types (Meyer et al., 2013). Floods are pointed out as the second most frequent extreme event in Brazilian municipalities between 1991 and 2012, with drought occupying the first place (CEPED/UFSC, 2013).

The analysis of land use and land cover in river basins is crucial for flood risk management, for supporting decision-making, flood forecasting and early warning systems, and for studying mitigating alternatives, among several other benefits (Paul et al., 2019; Ali et al., 2020). Flood risk mapping is a basic element for the design of mitigating strategies, justifying the regulation of this instrument by legislation as in the case of the USA and European countries (Degiorgis et al., 2012; Caldas et al., 2018). This type of mapping may also be adapted for evaluating flash floods, caused by the occurrence of rainfall with large volumes highly concentrated in time, or even due to the rupture of hydraulic structures such as dams (Arabameri et al., 2020).

Hydrological modelling is considered the most recommended approach to estimate flood areas, as it enables to mathematically represent the hydrological and hydrodynamic processes in the surface runoff generation and flood wave propagation, among other aspects, depending on the considered models. Thus, ideally, a distributed hydrological model can be combined to simulate the rainfall-runoff transformation process in areas contributing to the drainage network, and a two-dimensional hydrodynamic model to simulate the flood wave routing and floodplain inundation (Paz et al., 2011; Zambrano et al., 2020), or analogously for urban areas (Prakash et al., 2020), but there are several variants of this approach (Bravo et al., 2012; Pontes et al., 2017; Hdeib et al., 2018).

However, these mathematical modelling approaches require a considerable amount of field data and effort to process these data, to prepare and adjust the models (Lin et al., 2020), even with the avail-

ability of automation tools and the existence of graphical user interfaces (Siqueira et al., 2016). In addition, these approaches require considerable expertise in hydrological modelling that becomes incompatible with fast applications and expeditious surveys (Morelli et al., 2014). Alternatives have been developed by combining multiple layers in a geographic information system and using statistical analysis techniques, such as analytic hierarchy process, logistic regression and fuzzy logic, and machine learning methods such as artificial neural networks, decision trees and support vector machine (Degiorgis et al., 2012; Tehrany et al., 2015; Paul et al., 2019; Ali et al., 2020; Lin et al., 2020). At the same time, these approaches require in-depth knowledge of such methods, with a level of complexity that can discourage users and hinder their further application (Zheng et al., 2018a).

A more simplified alternative is the estimation of flood areas in a more expedient way, based on the processing of Digital Elevation Models (DEM) such as the method based on the terrain descriptor called HAND (Height Above Nearest Drainage) (Rennó et al., 2008). The proposal of this method is to produce reasonable estimates in a fast way, such as those required to prioritize evacuation areas during extreme events (Afshari et al., 2018), with an easy application procedure and requiring free widely available data for any area, taking advantage of the availability of DEM data (Garousi-Nejad et al., 2019). In fact, freely and globally available DEM, such as those from the SRTM Mission (Shuttle Radar Topography Mission) (Van Zyl, 2001), have been crucial for flood studies in places with low data availability (Hawker et al., 2018).

HAND is an information plan directly derived from DEM, involving two other products also extracted from DEM, namely the flow directions and the drainage network (Rennó et al., 2008; Nobre et al., 2011). The HAND concept, initially discussed in Rodda (2005) and named and presented as such by Rennó et al. (2008), is simple: each pixel or point of this information plane presents the altitude difference of this point in relation to the point of the drainage network to which it connects, according to the flow paths extracted from the DEM processing. To estimate flood areas based on HAND, according to the most simplistic approach, a certain height of this flood is assumed, and the HAND analysis is performed: all points of this layer that present attributes lower than the established flood height are considered flooded (Nobre et al., 2016). This method identifies flood areas assuming, therefore, that the water level equally rises along the entire river course, maintaining the unevenness along with the drainage network – that is, the water level rises parallel to the bottom of the river course.

Another benefit of the use of HAND as a flood area estimator is the continuous increase of available topographic data acquired by remote sensing, either showing improvements in terms of more refined spatial resolution, regarding the quality of the acquired information, or the removal of errors in already existing data (Hawker et al., 2018). For example, there are data available from new orbital sensors with

increasingly refined spatial resolution and other improved features such as the ALOS AW3D (Tadono et al., 2015), the ALOS PALSAR DEM (Niipele and Chen, 2019) and the TanDEM-X WorldDEM (Krieger et al., 2007). Another advantage is the availability of data resulting from improvements of already used DEM, such as MERIT (Yamazaki et al., 2017) and BEST (O'Loughlin et al., 2016), both proposed aiming at reducing the effect of vegetation and other noise on SRTM data, and EarthEnvDEM90, proposed as a fusion of SRTM and ASTER data (Robinson et al., 2014). Conversely, there is the increasing availability of data obtained from aerial or unmanned remote sensing, such as LiDAR survey data, which are already freely available for the entire state of Pernambuco, Brazil (Cirilo et al., 2014), or aerial photogrammetry data, such as those available for the state of Santa Catarina, Brazil (Momo et al., 2016), both with a refined spatial resolution of 1 meter.

In addition to applications for multiple purposes (Gharari et al., 2011; Nobre et al., 2011; Cuartas et al., 2012; Rahmati et al., 2018), several research studies have estimated flood areas based on HAND, comparing such studies with flood delineations estimated by remote sensing (Mengue et al., 2016; Garousi-Nejad et al., 2019) and analyzing them against field data indicating flood location and heights (Momo et al., 2016; Nobre et al., 2016; Goerl et al., 2017; Speckhann et al., 2018) or comparing them with estimates made by hydrological-hydrodynamic models (Momo et al., 2016; Afshari et al., 2018; Zheng et al., 2018b). Clement et al. (2018) and Landuyt et al. (2019) also report the use of HAND to mask and restrict areas estimated as inundated in studies on synthetic aperture radar images, either previously or as a post-processing step.

The effect of the channel initiation on the results of flood area estimates using HAND has also been evaluated (Mengue et al., 2016; Goerl et al., 2017; Speckhann et al., 2018) as well as the influence of the source of the DEM data (Zheng et al., 2018b) and the spatial resolution of the DEM (Goerl et al., 2017; Speckhann et al., 2018). Some studies have estimated flooded areas by proposing modifications to the HAND-based method, such as combining it with rating curves and streamflow forecasts (Liu et al., 2018; Zheng et al., 2018b; Garousi-Nejad et al., 2019) or with streamflow frequency analysis (Speckhann et al., 2018).

Despite the simple concept and the wide use of the HAND-based method, there are issues involved in the estimation of flood areas that require further study, which are addressed in this research:

- the effect of considering a spatially varying minimum area threshold to denote channel initiation, as this identification of the headwaters is one of the most challenging aspects in the DEM processing and has a strong influence on the extracted drainage network (Li et al., 2020), but no previous research considered such spatial variation in the computation of HAND;
- the impact of considering or not the depressionless DEM, taking into account that the removal of depressions is necessary

to establish continuity in flow paths and constitutes the main motivation in the improvement of DEM processing algorithms, although there are authors who used the DEM without depressions (Garousi-Nejad et al., 2019) and others who used the DEM with depressions (Zheng et al., 2018b) in the HAND calculation;

- evaluation of the hydrostatic condition of the flood area, preliminarily mentioned by Momo et al. (2016);
- the effect of incorporating an existing vector network as a DEM pre-processing procedure (Lindsay, 2016), deepening the related discussion as the one presented by Mengue et al. (2016);
- comparative analysis of HAND-based results to the basin morphology in terms of the longitudinal profile of rivers.

This study aims to verify the applicability of HAND in estimating flood areas, covering the five raised issues and deepening the understanding of such approach. The Mamanguape River basin, located in the state of Paraíba (Brazil) and subject to a historical record of flash floods and serious consequences (Aagisa, 2004), is considered as the study area.

Materials and Methods

Study area and data

The study area, the Mamanguape River basin, is located entirely in the state of Paraíba, in Northeast Brazil, in the mesoregions of Zona da Mata and Agreste, and with a drainage area of 3,522.7 km² (Governo do Estado da Paraíba, 2006; Figure 1). A warm and wet climate predominates in the region, with the main rainy period between March and August and annual precipitation ranging from 700 to 1,600 mm (Barbosa, 2006; Santos et al., 2015). The Atlantic Forest biome predominates in this basin, with the presence of *restinga* and mangrove vegetation (Rodrigues et al., 2005).

The Mamanguape River basin is the third largest basin in the state of Paraíba in terms of area and has a fundamental role in economic, social, and environmental aspects, especially for over 42 municipalities totally or partially inserted in this area. Ten of these municipalities are in areas prone to the occurrence of river flooding (Aagisa, 2004; Barbosa, 2006), with a total population of over 450,000 inhabitants (Santos et al., 2015).

The topography varies from sea level at the river mouth in the east region to 750 m in the Borborema Plateau region (Marques et al., 2015). Topographic variation, characteristics of the rainfall regime, and geomorphological characteristics of the basin increase the occurrence of flash floods, in response to intense precipitation events, with rapid runoff and large destructive power. In 2004, one of these flash flood events occurred, with major socioeconomic losses (Aagisa, 2004). A field survey during the flood identified more than 150 critical points in the basin (Aagisa, 2004; Figure 1).
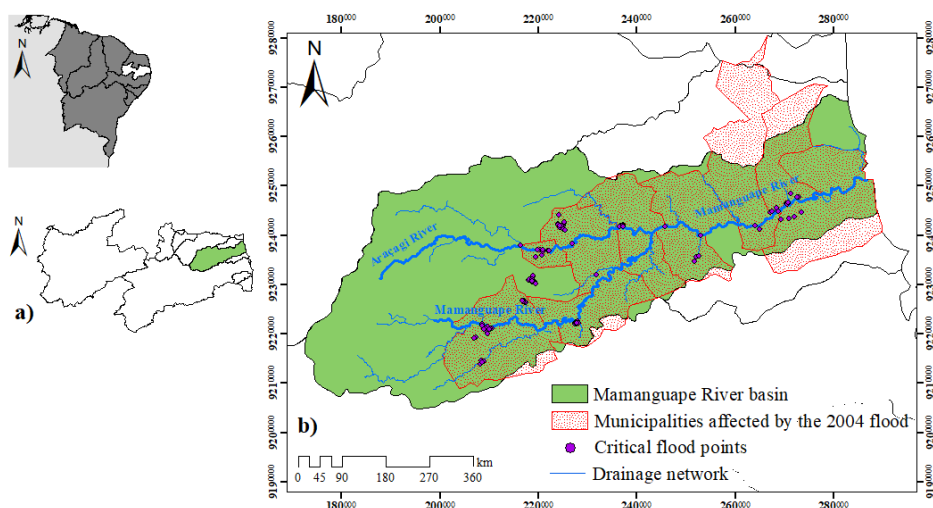
Figure 1 – (A) Location of the Mamanguape river basin in the state of Paraíba, Brazil and (B) Delimitation of the basin with the indication of the drainage network and critical flood points raised for the 2004 event according to Aagisa (2004).

In addition to this field survey of the critical flood points in the 2004 event, the materials used for the present research were: DEM with spatial resolution of 30 m from SRTM data (Farr et al., 2007); vector river drainage network available from the geographic data portal of the Paraíba State Water Resources Management Executive Agency (*Agência Executiva de Gestão das Águas do Estado da Paraíba – AESA*); and satellite images available from Google Earth.

Basic Digital Elevation Model processing

The DEM of the study area was initially processed to derive basic information layers for estimating flood areas. Depressions were removed and flow directions were defined, i.e., the flow direction for each pixel was established in the direction of one of its eight neighbors (D8 method –Deterministic Eight-Neighbor; Mark, 1984; Jenson and Domingue, 1988). Depressions that were removed can be either real, such as areas of the terrain lower than the neighborhood, or artefacts caused by noise and other interference during DEM data acquisition (Barnes et al., 2014). This removal of depressions is necessary to achieve flow path continuity from the headwaters to the basin mouth (Mark, 1984; Jenson and Domingue, 1988).

The main rule for defining flow direction is to set this direction toward the neighboring pixel that provides the highest slope, but with specific rules for the treatment of situations of depressions and flat areas according to each algorithm, usually involving operations of elevation increase or decrease (Barnes et al., 2014). The TerrSET software was used, whose algorithm for removing depressions and defining flow directions is of the Priority First Search type (PFS;

Sedgewick, 1992; Jones, 2002), described by Buarque et al. (2009) and Siqueira et al. (2016) with results evaluated as of superior quality in relation to other algorithms, such as the one used in the ArcGIS software, which tends to present unreal parallel drainage lines (Paz and Collischonn, 2008).

The accumulated drainage areas were determined based on the flow directions. These areas consist in a raster layer whose attribute of each pixel represents the upstream contribution area (sum of the areas of the pixels whose flow paths drain into the pixel in question). Based on the definition of the Mamanguape River basin outlet into the ocean, the river basin was delimited by the automatic identification of all pixels whose runoff drains into this point.

Drainage network determination

The drainage network was determined based on the accumulated drainage areas, initially following the procedure of adopting a uniform minimum threshold (Amin) of accumulated area (Fan et al., 2013; Momo et al., 2016; Goerl et al., 2017; Speckhann et al., 2018). In other words, all pixels in the river basin that have drainage area greater than Amin become representatives of the drainage network. Different Amin values were adopted to represent the sensibility of the drainage network obtained to this parameter: 5, 10, 25, 50, 75, and 100 km², resulting in their corresponding drainage networks.

This procedure is simplified, considering that physical (soils, vegetation cover, relief, geology, etc.) and climatic (precipitation) characteristics imply that each headwater formation corresponds to

a specific upstream accumulated area. Hence, a second procedure was adopted, considering a spatially variable Amin value, following the approach suggested by Fan et al. (2013). Based on satellite images available from Google Earth, 25 headwaters of the drainage network were visually identified and the drainage area value derived from the DEM corresponding to each of these points was surveyed. Based on these values, the basin was divided into three regions considered relatively uniform regarding the upstream drainage area of the surveyed headwaters. For each region, a specific Amin value was adopted (20.54 km², 39.92 km², and 78.75 km²), established by the average of the accumulated area identified for the headwater points in the region.

Incorporation of the existing vector drainage network

Considering the river vector drainage network provided by AESA and assuming that one intends to determine flow paths from the DEM in a compatible way with such vector network, the DEM pre-processing procedure known as stream burning was performed (Lindsay, 2016; Wu et al., 2019). The vector network was converted to a raster format, with the same spatial resolution of the DEM, and them the decrease of the elevation of DEM pixels located exactly along the representative pixels of the vector network was performed. This burned DEM was processed to remove depressions and derive flow directions, accumulated areas, river basin delimitation, and drainage network, as described in the previous items for the DEM without stream burning.

Extracting the longitudinal profiles of the drainage network

A computational routine in FORTRAN language was developed to elaborate longitudinal profiles of the entire river drainage network, with the following algorithm:

- starting from each headwater, the downstream flow path is followed pixel by pixel according to the flow directions;
- the accumulated distance travelled (Dacum_i) is counted, where each incremental step between pixels has summed the size of a pixel (dx) or the value of $\sqrt{2}dx$, if the step is orthogonal or diagonal, respectively;
- the elevation of the visited pixel (Z_i) is recorded;
- after following all flow paths, the distance of each pixel relative to the basin outlet (Dexu_i) is calculated as the difference between Lmax and Dacum_i, where Lmax is the full river length relative to the outlet.

The pairs of points (Dexu_i, Z_i) are considered to construct the longitudinal profiles. As the distances in each profile were calculated in relation to the basin outlet, it is possible to graph all points of the drainage network together, increasing the potential of the analysis.

HAND determination

For determining the HAND terrain descriptor, another computational routine was developed in FORTRAN language, having as input the DEM, the flow directions, the basin delimitation, and the drainage network in the raster format. For each pixel of the basin that is not part of the drainage network, its elevation (Zp) is registered and the downstream flow path until reaching the drainage network is traced, registering the elevation of this pixel of the drainage network (Zr) that was reached. HAND is calculated by the difference between Zp and Zr, that is, the topographic referential of HAND varies (Nobre et al., 2016), and each pixel has its corresponding referential (Zr).

The routine execution was repeated, and several HAND layers were obtained, varying one or more of the input data (Table 1), to provide three main focuses of comparative analyses. For the first analysis, HAND was determined considering the drainage network obtained from the uniform Amin rule, but testing different values (HANDu5 to HANDu100), and considering the drainage network obtained from the spatially heterogeneous Amin (HANDhet). All other input data for HAND remained unchanged for this first analysis.

The second analysis was performed with two configurations for obtaining HAND that only differs to the input DEM: one configuration uses the original DEM, from SRTM-30m data, which presents depressions as any DEM without pre-processing (HANDdep); the other configuration uses this DEM after having the depressions removed for generating continuous flow paths (HANDhet). In the third analysis, the difference between both configurations for obtaining HAND is only the flow directions and, consequently, the derived drainage network: in one configuration, the flow directions were obtained by applying the PFS algorithm of TerrSET to the depressionless DEM determined from SRTM-30m data (HANDhet); in the other configuration (HANDburn), this same algorithm for determining the flow directions is employed, but firstly the SRTM-30m DEM is pre-processed with the incorporation of the drainage vector network made available by AESA (stream burning procedure).

Estimation of flood areas

For each HAND configuration, the estimation of flood areas was performed in the standard way, by adopting an inundation height threshold. In other words, once this threshold (Hlim) is established, all pixels with HAND attribute lower than Hlim are part of the flood area. Different arbitrarily chosen Hlim values were tested to denote a variation of the flood height, and the Hlim value of 1.5 m was also specifically evaluated based on information reported for the flood height that occurred in the 2004 event (Folha de S. Paulo, 2004).

For estimating the flood areas obtained from the HAND configuration adopted as reference (HANDhet), the inclusion of a post-pro-

Table 1 - Configurations used for the determination of the different HAND layers and an indication of the main focus of each comparative analysis.

Pre-processing the DEM to obtain flow directions (stream burning)	Input DEM for HAND	Amin's criterion for obtaining drainage network		HAND	Comparative analysis	
No	DEM without depressions	Uniform Amin	5 km²	HAND$_{u5}$	Influence of the drainage network initiation	Stream-burning effect
			10 km²	HAND$_{u10}$		
			25 km²	HAND$_{u25}$		
			50 km²	HAND$_{u50}$		
			75 km²	HAND$_{u75}$		
			100 km²	HAND$_{u100}$		
		Heterogeneous Amin		HAND$_{het}$		
	DEM with depressions	Heterogeneous Amin		HAND$_{dep}$	Effect of considering the removal of depressions	
Yes	DEM without depressions	Heterogeneous Amin		HAND$_{burn}$		

cessing step was additionally evaluated to impose the hydrostatic condition in the immediate neighborhood of flood areas.

In a situation of a flood area in which the velocity of water can be neglected, pressure at any point of this region follows the hydrostatic approximation. Considering that the variation in water density is also negligible, according to this hydrostatic approximation, pressure is a function of the height of the water level above the considered point. In this study, it was verified whether, for each pixel integrating the flood area, there was a valid hydrostatic equilibrium condition concerning the neighboring pixels.

The procedure was carried out as follows: for each flooded pixel, the authors identified which of its eight neighbors in a 3x3 window were not flooded; for each non-flooded neighbor, it was checked whether its elevation was lower than the sum of the elevation and the height of the water level in the central flooded pixel. If this was the case, the hydrostatic condition was not satisfied, and the neighboring pixel was considered flooded.

Results and discussion
Estimation of flood areas: configuration of the reference HAND

With the HAND configuration considered as reference (HAND-het), the terrain descriptor varied over the Mamanguape River basin as illustrated in Figure 2A, with a predominance of lower values near the drainage network, mainly in the middle and lower parts of the basin, as expected. By assuming a 5-m HAND threshold, the corresponding flood areas are predominantly in the margins of the watercourses, with greater spreading in the final stretch of

Mamanguape River near the basin outlet. Nevertheless, there are also regions in the upper and middle parts of the basin, including marginal areas toward the Araçagi River and, in lower proportion, in smaller tributaries (Figure 2B).

The total flood area obtained ranged from 10.7 km², for the 1-m HAND threshold considered as flood height, to 404.7 km², when considering 15 m for such threshold (Figure 3A). An increase in flood area as a function of the increase in flood height based on HAND is noted, approximately following a third-degree polynomial function, a pattern similar to that found by Goerl et al. (2017) for another study area. The result presented in Figure 3A refers to the spatially variable Amin threshold condition for obtaining the drainage network (Figure 3B), as described by the HANDhet configuration in Table 1.

Influence of the definition of the drainage network initiation

By varying the criteria for defining the drainage network initiation, a direct effect is produced on the total flood areas estimated based on HAND, for the same flood height threshold of 5 m (Figures 3B and 4).

With a uniform minimum area equal to 5 km², there is an estimate of 166.7 km² of flood areas, a total that exponentially decreases to 77.3 km² (54% reduction) when considering a uniform minimum area of 100 km². This result pattern of inundated area reduction as a function of increasing Amin parameter was also obtained by other authors (Mengue et al., 2016; Goerl et al., 2017; Speckhann et al., 2018) for other study areas. This may be generalized and expected for any area considering that, conceptually, there is a reduction of the drainage
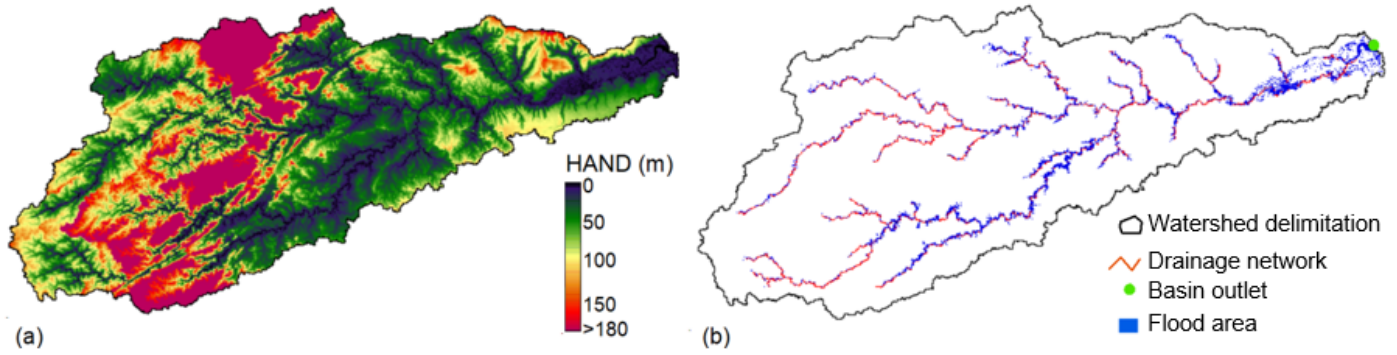
Figure 2 – (A) HAND terrain descriptor obtained for the HANDhet configuration; (B) Flood area assuming a 5-m HAND threshold and the HANDhet configuration.
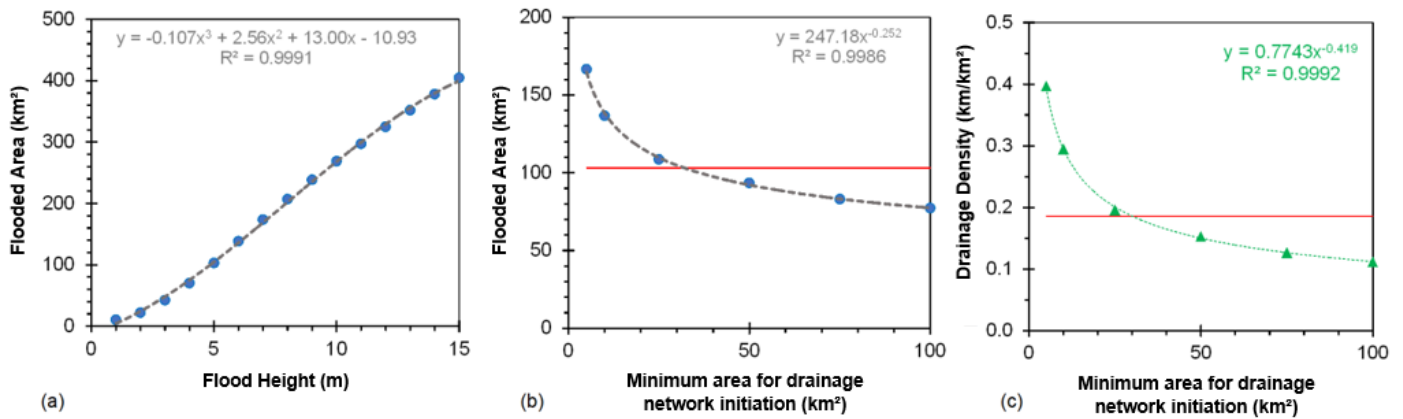

Figure 3 – (A) Flood height used as HAND threshold and the corresponding obtained inundated area (HANDhet configuration); (B) Minimum area for drainage network initiation and the corresponding obtained inundated area, considering a 5-m HAND threshold; (C) Minimum area for drainage network initiation and the resulting drainage density; the red line indicates the value on the y-axis for a spatially variable minimum area, whereas the dashed curves and equations indicate the trend curves fitted to the points.
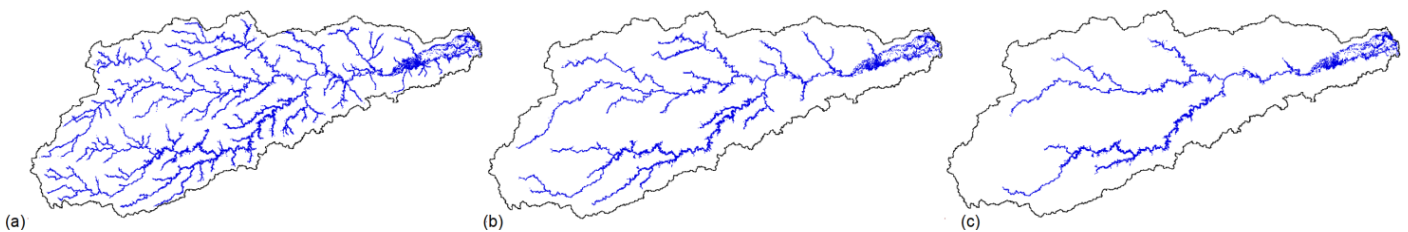

Figure 4 – Mapping of flood areas for a 5-m HAND threshold, considering a uniform minimum contributing area for drainage network initiation with values of (A) 5 km² (HANDu5); (B) 25 km² (HANDu10); and (C) 100 km² (HANDu100).

network extension with the increase in the minimum area and, consequently, the drainage density. In the Mamanguape River basin, for a minimum area of 5 km², there is a total of 1,311 km of rivers in the basin (drainage density of 0.40 km/km²), whereas the total extension is only 371 km (drainage density of 0.11 km/km²) when considering a minimum area of 100 km².

In the study conducted by Mengue et al. (2016), the comparison of the results obtained from HAND considering different values of

Amin with the estimate of the inundated area from LANDSAT satellite images allowed identifying which Amin value provided the better agreement. However, it is understood that the estimate based on HAND could be further improved if the spatial variability of Amin was incorporated. The consideration of a spatially variable minimum area for the drainage network initiation is a more reasonable way for obtaining the drainage network and it has greater resemblance to reality than assuming a uniform value, as there is no uniformity in the drainage area of each river headwater.

In the study by Liu et al. (2018), the location of the identified headwaters of a reliable vector network representative of the river course was used as the definition of the DEM-derived drainage network initiation. This ensures not only the issue of each headwaters with their specific contributing area, but also increases the reliability of this DEM-derived drainage network, proportionally to the quality of the available vector network. But this approach is clearly limited to the availability of this vector network of acceptable quality. Meanwhile, McGrath et al. (2018) adopted the criterion of applying HAND only considering the reaches of the drainage network with higher order according to the hierarchy of the Strahler method. However, this approach does not disregard the effect of the Amin choice to denote the drainage network initiation. In fact, the channel initiation influences the hierarchy of the network according to the Strahler method. Furthermore, there is the subjectivity of which minimum hierarchical order of the drainage network to be adopted for HAND determination.

An alternative would be to identify the drainage network initiation from the combination of the contribution area (A), the local slope (S), and a parameter k by the expression AS^k, as adopted by Degiorgis et al. (2012). This method would also lead to spatial heterogeneity of the contributing area at each of the headwaters, but with the disadvantage of involving an additional parameter (k), in addition to

the decision of which threshold to adopt for the AS^k term denoting the channel initiation.

With the Amin parameter spatially varying as performed in this study, a total river length equal to 615 km was obtained (drainage density of 0.19 km/km²) and the inundated area for the 5-m HAND threshold was 103.1 km² – results that are close to those obtained for the uniform condition of the minimum area equal to 25 km². However, the spatial occurrence of the flood areas presents considerable differences between the two cases. This is because, when considering the spatially variable minimum area, there is a change in the positioning of each headwater concerning the drainage generated by considering a constant minimum area. This variation is even greater when comparing the results obtained from the variable minimum area with those obtained for the other minimum area values (Figure 4).

Effect of the removal process of DEM depressions

In order to obtain the continuous flow paths downstream from any pixel of the basin up to the outlet, depressions that reached 3.1% of the river basin pixels were removed. Most of them (84% or 2.6% of the river basin total) resulted from elevation lowering; and the remaining (16% or 0.5% of the river basin total), from elevation raising. Most of the removed depressions are located along with the drainage network and are associated with the effect of the vegetation marginal to the river on SRTM data (O'Loughlin et al., 2016). This leads to the difference among the longitudinal profiles drawn along the Mamanguape River considering the original DEM (with the presence of depressions) and the depressionless DEM (Figure 5A).

The removal process of depressions tends to generate lower elevations than there were in the original DEM along the main river, in addition to smoothing the elevation variations. Considering that the effect of vegetation on the elevations in the SRTM data and the abrupt
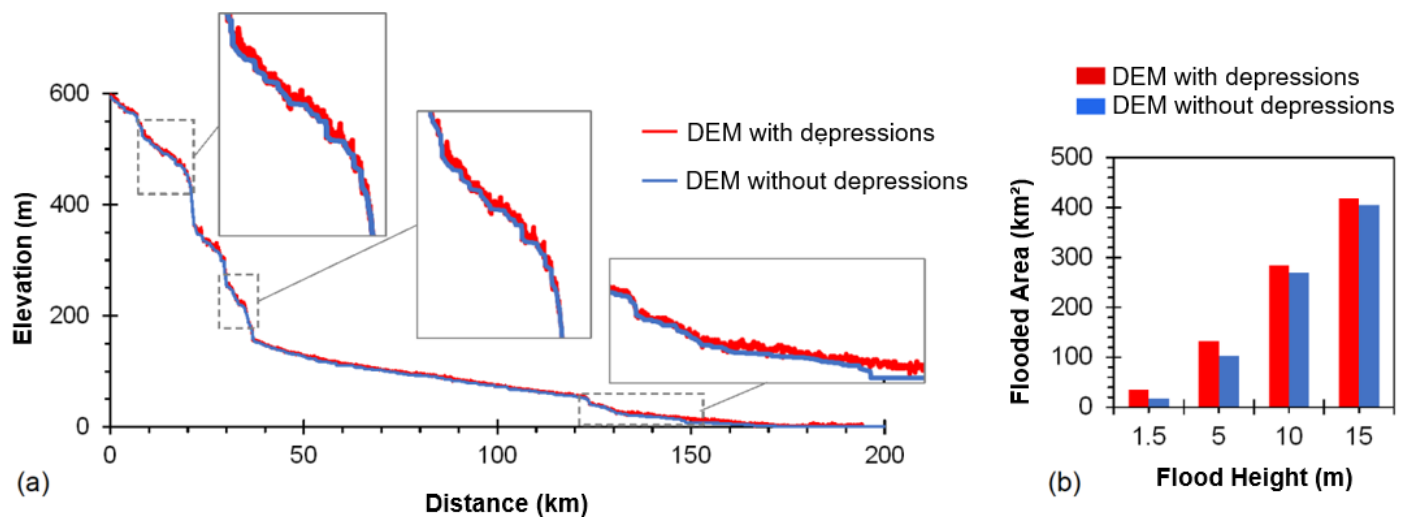

Figure 5 – (A) Mamanguape River longitudinal profile considering DEM with and without depressions; (B) Inundated area in the basin for different flood heights considering DEM without and with depressions, in the HANDhet and HANDdep configurations, respectively.

variations in elevation along the main river are not consistent with reality, it is more reasonable to consider the DEM without depressions as input for the HAND calculation, as used by Garousi-Nejad et al. (2019), than the original DEM with depressions (adopted by Zheng et al., 2018b). However, to minimize the effect of the removal of depressions, Garousi-Nejad et al. (2019) adopted a procedure that relies on elevation information from another data source, with higher spatial resolution. This is a methodological alternative, though limited to the availability of such auxiliary data. Zheng et al. (2018b) evaluated, as an advantage of using the DEM with depressions, the fact of correctly identifying local flood areas, such as small lakes not connected to the drainage network, from the comparison with estimates made by hydrological modelling.

In this research, the lower elevations present in the depressionless DEM along the main river induced higher HAND values for other points in the basin and the reduction of flood areas for the same HAND threshold, compared with the use of the original DEM (Figure 5B). This reduction ranged from 3% to 99% according to the HAND threshold, with greater difference the lower the considered flood height. This indicates a greater impact of considering DEM with or without depressions on the estimation of flood areas corresponding to smaller floods. In this type of event, flood areas are predominantly in the parts of the floodplain closest to the river channel, precisely the regions most subject to vegetation height bias on the SRTM data. This is because vegetation affects the elevations of the SRTM DEM (O'Loughlin et al., 2016; Yamazaki et al., 2017), and there is greater presence of vegetation in areas marginal to the rivers in the studied basin.

This pattern of results becomes clearer when observing the map with values concerning differences between the HAND obtained for the DEM with depressions (HANDdep) and that without depressions (HANDhet). Negative values are predominant (Figure 6A), indicating that HANDhet presents higher values than HANDdep. In the comparison of the flood areas corresponding to the 5-m HAND threshold, the

consideration of the DEM with depressions leads to the identification of more areas subject to flooding in the lower part of the basin than the DEM without depressions, but this also occurs in a lower proportion in the middle and upper parts (Figure 6B).

Comparative analysis of the morphology of the basin concerning the longitudinal profile of the rivers

When generating the drainage network from the accumulated areas, by considering the criterion of a spatially variable minimum contributing area to denote the drainage network initiation, that is, considering the value of the parameter Amin variable in the basin, 31 headwaters were obtained (Figure 7A). For each drainage headwaters, the area directly contributing to the continuous river reach downstream of that point was also identified, whereas the longitudinal profiles of these reaches are presented in Figure 7B, maintaining the basin outlet as a reference of the distances in the x-axis.

Headwater 1 represents the channel initiation of the main river of the basin, which is the Mamanguape River, whose points every 10 km of distance are indicated in Figure 7C. In the longitudinal profile of this river there is an abrupt variation in slope around 165 km from the outlet. This has a direct impact on the occurrence of larger flood areas downstream to this point than along upstream reaches of this river (Figure 7D). The figure illustrates the extent of incremental flood areas (i.e., not cumulative) directly connected to each point along the Mamanguape River. An abrupt change is verified around the 165-km position, with greater occurrence of flood areas than in previous positions. This is a coherent result, as this abrupt change in the longitudinal slope of the river drastically alters its hydraulic conveyance, resulting in a lower capacity of the river to convey the flow, which facilitates the overflow of the river channel onto the floodplain. In fact, in the field survey carried out for the 2004 flood (Figure 1), several points of the overflow of the channel and floodplain inundation were observed along this river reach.

(a)

Difference in HAND (m)
< -10
-5
0
5
> 10

(b)

Flood area
■ Only for DEM without depressions (HANDhet)
■ Only for DEM with depressions (HANDdep)
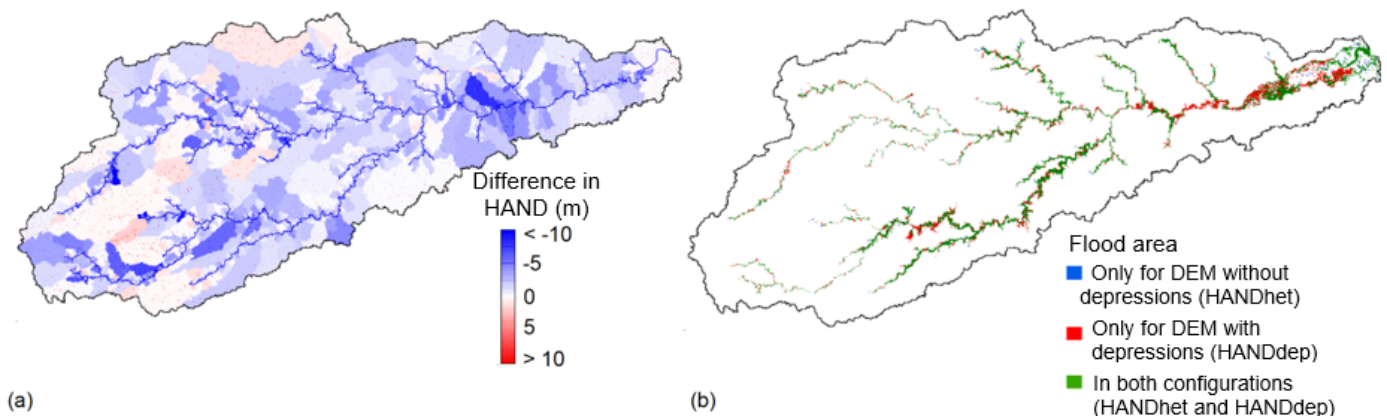■ In both configurations (HANDhet and HANDdep)

Figure 6 – (A) Difference in HAND obtained from the DEM with depressions and the DEM without depressions; (B) Analysis of flood-prone areas obtained only from the DEM without depressions, only from the DEM with depressions, and those simultaneously obtained from both.

Around the 55-km position, an increase in riverbed slope reduces the occurrence of flood areas, whereas around the 40-km position there is another remarkable reduction in slope, once again increasing the occurrence of flood areas.

Effect of the stream burning procedure

The vector drainage network provided by AESA presents some divergences compared with the drainage network obtained in this research from the SRTM DEM data, mainly in the lower part of the basin near the outlet (Figure 8A). The AESA vector drainage network was used for pre-processing the SRTM DEM data by the stream burning procedure, in such a way to obtain the flow paths and the raster drainage network. With these data, HAND (HANDburn) was obtained, whose difference in relation to the reference HAND of this study (HANDhet) indicates that the DEM pre-processing by stream burning has resulted in the decrease of the HAND in most of the basin (Figure 8B). As a result, there is an increase in the flood areas obtained from HANDburn in relation to HANDhet, and such increase is distributed throughout the extension of the drainage network, but with a higher concentration in the lower part (Figure 8C).

The procedure used for HANDburn was similar to the procedure adopted by Mengue et al. (2016), and aims at producing results compatible with an existing river drainage network. This is indeed the benefit reported in the literature when using the stream burning procedure (Lindsay, 2016; Wu et al., 2019). But such compatibility occurs in terms of the river drainage network as such, i.e., the network derived from the DEM modified by stream burning approximates the existing vector network. It is understood that this is valid if the existing vector drainage network is representative of the actual river flow paths, at least in higher quality than the flow paths resulting from the DEM processing, as in the case of the application of HAND made by Garousi-Nejad et al. (2019). If there are no elements to measure the quality of the available river vector network, the performance of the stream burning processing is deemed unreasonable.

Conversely, even if the quality of the available vector drainage network is guaranteed, the use of such vector network for DEM pre-processing by stream burning prior to obtaining the HAND is questionable for two reasons.
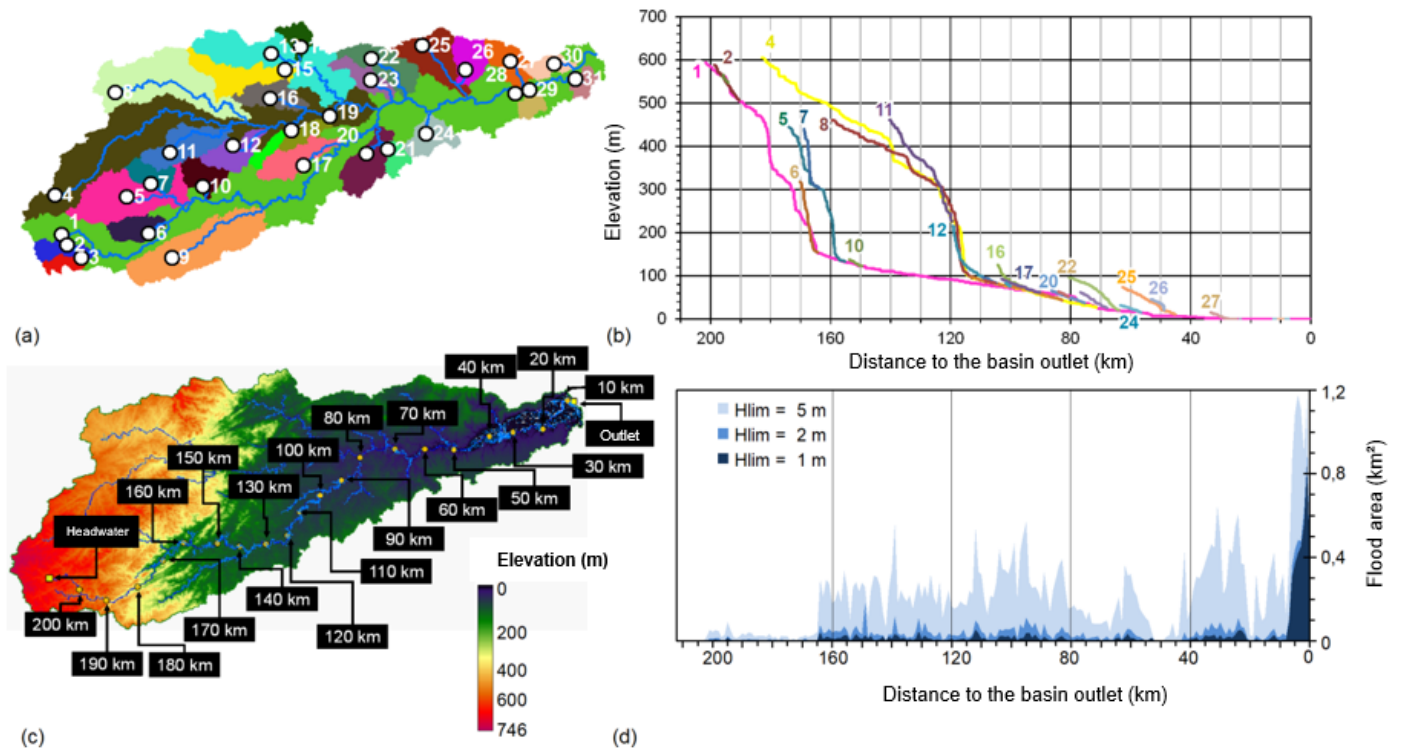

Figure 7 – (A) Identification of the 31 headwaters of the drainage network and the corresponding areas of direct contribution to the continuous downstream river reach; (B) Longitudinal profiles of each river reach downstream of the headwaters, with distance measured to the basin outlet and numerical identification of the main headwaters; (C) Digital Elevation Model with indication of the accumulated distance along the Mamanguape River, measured from the basin outlet, according to each yellow dot mark; (D) Incremental flood area at each specific point of the Mamanguape River, in HANDhet configuration and for three HAND thresholds.
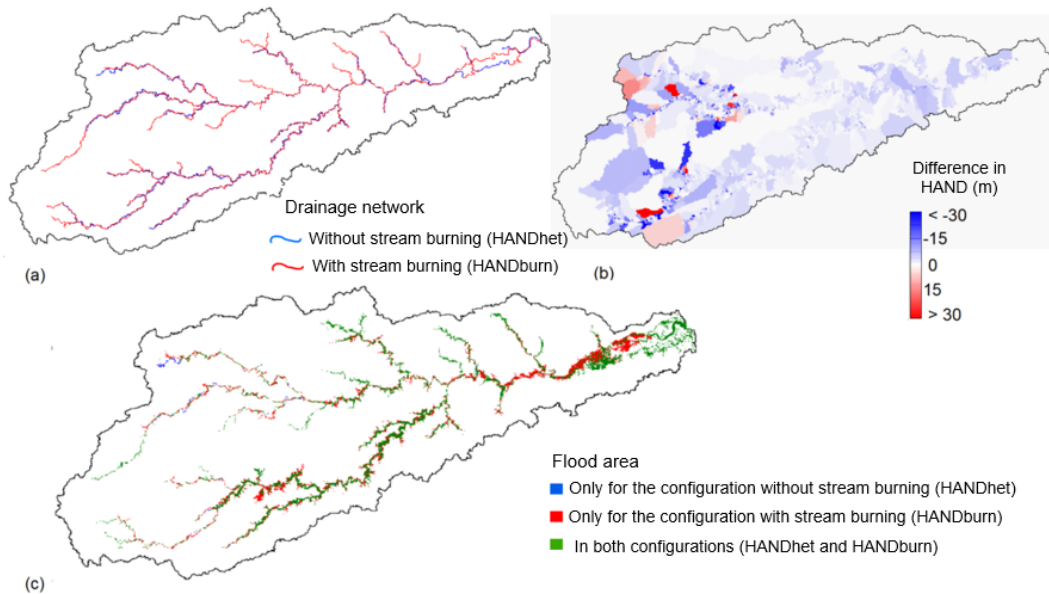
Figure 8 – (A) Comparison between river drainage networks obtained with and without stream burning; **(B)** Difference in HAND obtained using the DEM with and without stream burning; **(C)** Analysis of flood areas obtained only for HAND without stream burning, only for HAND with stream burning, and simultaneously obtained with both.

First, it is assumed that the burned DEM should not be used to calculate HAND, as it presents elevations arbitrarily lowered along with the drainage network, which was not done in this research and is addressed in the literature (Mengue et al., 2016). Garousi-Nejad et al. (2019) present another point of view, whose results showed that the lowering of the DEM according to the vector drainage network led to greater coherence of the flood area estimates compared with hydrological modelling studies. In the aforementioned study, by having a vector drainage network that is well representative of the river course and having a high spatial resolution DEM, the lowering of the DEM by stream burning prevented large areas marginal to rivers from being erroneously identified as flooded areas. The burning procedure also avoided inconsistencies in the results caused by bridge interference in the DEM, which exemplifies the high spatial resolution of the DEM used by the authors. Nevertheless, in studies such as the present one, which use DEM from SRTM data and have an available vector network whose degree of concordance with the river course is unknown, stream burning would not present this advantage.

Second, there is the conceptual issue of compatibility of the topographic information from the DEM with the available vector network. The use of flow directions and drainage network derived from the burned DEM, as input to obtain HAND, leads to results of this terrain descriptor inconsistent with the morphological pattern represented in the DEM. This occurs because the DEM was modified by stream burning only in the pixels along that vector trace.

However, by not applying the stream burning, the results of HAND and estimated flooded areas may be spatially incoherent in relation to the actual drainage network delineation. An alternative is to improve the acquisition of DEM data itself so that their processing better represents the actual drainage network, as in the case of Garousi-Nejad et al. (2019). These improvements may include the refinement of the spatial resolution of the DEM (as pointed out by Speckhann et al., 2018; Goerl et al., 2017 and Garousi-Nejad et al., 2019) and reduction of noise and other interferences such as vegetation cover. The quality of the topographic data source is pointed out as key information for estimating flood areas, including when using more elaborate methods such as hydrodynamic modelling (Zambrano et al., 2020).

Hydrostatic condition analysis

The hydrostatic condition of the flooded area, with estimation results based on HAND, is addressed in this topic, considering the HANDhet reference configuration. For instance, consider the pixels Pa, Pb, and Pc indicated in Figure 9A, whose elevation is the same (57 m). According to the flow paths illustrated in Figure 9B, pixels Pb and Pc drain into the same point in the drainage network, whose elevation is 50.9 m, which is distinct from the point to which the flow drains from pixel Pa, whose elevation is 52.4 m. As a result, the HAND of Pa is 4.6 m, whereas the HAND of Pb and Pc is 6.0 m (Figure 9C). When considering a 5-m HAND threshold for identifying the flood area, Pa is part of the flood area, but Pb and Pc are not

(Figure 9D), thus violating the hydrostatic condition of this flood area delimitation.

All green pixels in Figure 9E are not considered to be inundated by the HAND criterion, but are immediate neighbors to pixels in the inundated area and have elevation equal to or lower than those inundated. The orange pixels consist in those neighboring the immediate neighbors to the HAND-based flood area, but they also meet the elevation criterion and would thus be flooded as well. By doing this procedure for the entire Mamanguape River basin, there is an increase in the flood area of 2.18 km² and 1.19 km², respectively, for the regions of the immediate neighborhood and second neighborhood to the inundated area by the direct HAND criterion. These are small increases, representing 2.1% and 1.2%, respectively, of the flood area according to the HAND threshold. Thus, although the isolated HAND criterion does not guarantee the hydrostatic condition in the neighborhood of each pixel considered part of the inundated area, despite what Momo et al. (2016) states, the inclusion of areas to guarantee such condition increased this inundate area in a practically negligible way in this study.

Conclusions

In this research, the HAND terrain descriptor was applied to the Mamanguape river basin for estimating flood areas, obtaining the following conclusions:

- The definition of the drainage network initiation controlled its extension and density, which altered the HAND values and, consequently, the estimation of flood areas. Adopting a uniform minimum area value to denote the drainage network initiation is a simplification that continued to have a considerable effect on the estimation of flood areas based on HAND, regardless of the value of this parameter. Ideally, the spatial variation of this parameter over the basin should be adopted or the location of the headwaters should be previously identified;

- In the HAND calculation, the choice of using the original DEM or the DEM modified by the removal process of depressions impacted on the results concerning flood areas, mainly for minor flood heights. It is recommended to consider the DEM without depressions, as this leads to a smoothing of the longitudinal flood profile along the river, which is more consistent with reality, rather than there being sharp variations in flood elevation due to point variations in river bottom elevation;

- The estimate of flood areas based on HAND is coherent with the basin morphology expressed in terms of the topographic longitudinal profile of the river. Widespread occurrence of flood areas was clearly associated with sudden reductions in the river slope pattern, due to an abrupt reduction in hydraulic conveyance and greater chance of runoff overflow to the floodplain. The analysis of the total of flood areas connected by the DEM-derived flow paths to each point along the river course was essential for this type of verification;
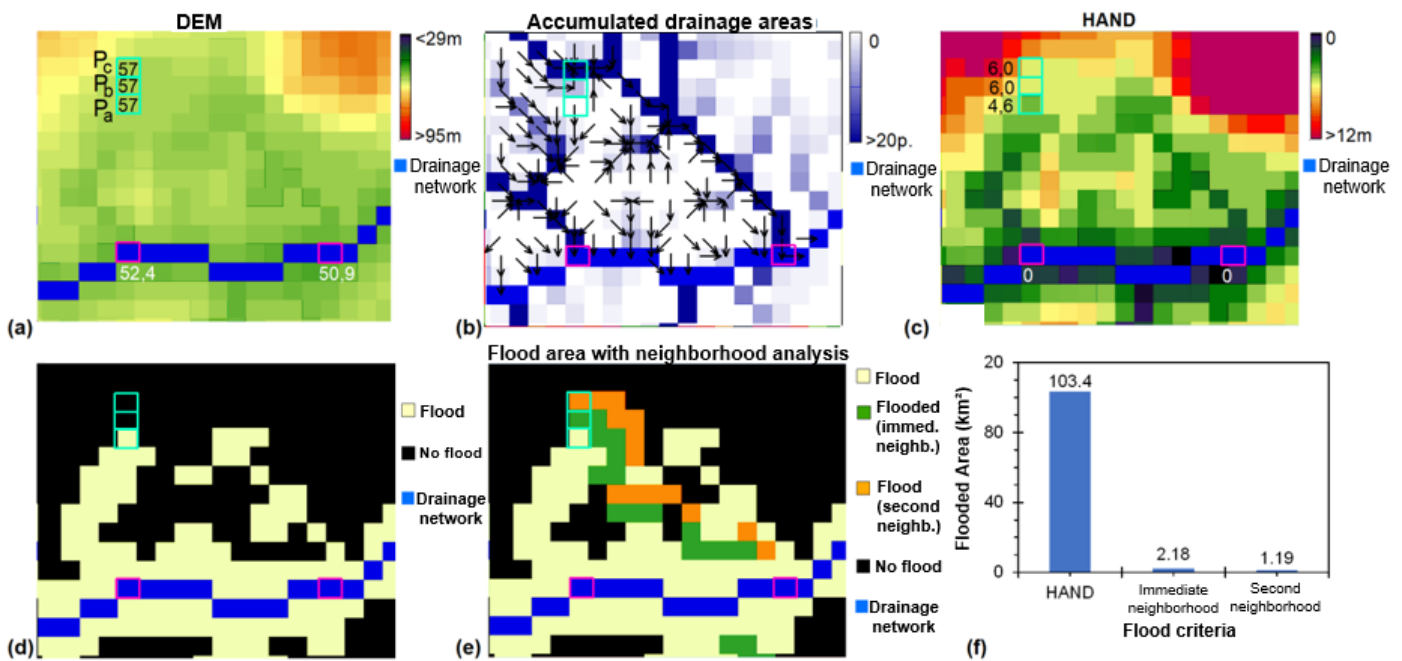

Figure 9 – Analysis of the hydrostatic condition of the flooded areas based on HAND: (A) DEM; (B) Accumulated drainage areas, with indication of the flow directions by arrows; (C) HAND – HANDhet configuration; (D) Flood area for 5-m HAND threshold; (E) Flood area with neighborhood inclusion; (F) Total flooded area obtained from the HANDhet configuration and by the additional criteria of immediate neighborhood and second neighborhood.

- The incorporation of an existing drainage network as a DEM pre-processing step (via stream burning) induced the network derived from the DEM to become more compatible with such existing network, though causing inconsistencies in the HAND method regarding the morphological pattern represented in the DEM. As a solution, there is the improvement of the DEM data acquisition, in such a way to better represents the drainage network trace;
- The hydrostatic condition did not occur in the flood areas estimated from the HAND, with sets of no flood pixels that have the same elevation or even lower elevations than neighbors integrating the flood areas. However, this occurrence was in a quantity that can be disregarded in terms of the impact on the pattern of flood estimates in this basin;
- Finally, it is recommended to validate the results of this research by applying the methods used to estimate flood areas for a specific actual flood event in the Mamanguape river basin, estimating the inundated area from field observations or, at least, via other tools such as satellite images or hydrodynamic modelling.

Contribution of authors:

Dantas, A.A.R.: Literature review, Data preparation, Methodology, Investigation, Writing. Paz, A.R.: Conceptualization, Literature review, Methodology, Investigation, Writing.

References

Aagisa, V., 2004. Relatório sobre a elaboração do mapa de inundações: Bacia do Rio Mamanguape. João Pessoa.

Afshari, S.; Tavakoly, A.A.; Rajib, M.A.; Zheng, X.; Follum, M.L.; Omranian, E.; Fekete, B.M., 2018. Comparison of new generation low-complexity flood inundation mapping tools with a hydrodynamic model. Journal of Hydrology, v. 556, 539-556. https://doi.org/10.1016/j.jhydrol.2017.11.036.

Alfieri, L.; Bisselink, B.; Dottori, F.; Naumann, G.; De Roo, A.; Salamon, P.; Wyser, K.; Feyen, L., 2017. Global projections of river flood risk in a warmer world. Earth's Future, v. 5, (2), 171-182. https://doi.org/10.1002/2016EF000485.

Ali, S.A.; Parvin, F.; Pham, Q.B.; Vojtek, M.; Vojteková, J.; Costache, R.; Linh, N.T.T.; Nguyen, H.Q.; Ahmad, A.; Ghorbani, M.A., 2020. GIS-based comparative assessment of flood susceptibility mapping using hybrid multi-criteria decision-making approach, naïve Bayes tree, bivariate statistics, and logistic regression: A case of Topľa basin, Slovakia. Ecological Indicators, v. 117, 106620. https://doi.org/10.1016/j.ecolind.2020.106620.

Arabameri, A.; Saha, S.; Chen, W.; Roy, J.; Pradhan, B.; Bui, D.T., 2020. Flash flood susceptibility modelling using functional tree and hybrid ensemble techniques. Journal of Hydrology, v. 587, 125007. https://doi.org/10.1016/j.jhydrol.2020.125007.

Barbosa, F.A.R., 2006. Medidas de proteção e controle de inundações urbanas na bacia do rio Mamanguape/PB. Master Thesis, Mestrado em Engenharia Urbana, Universidade Federal da Paraíba, João Pessoa. Retrieved 2020-06-24, from www.repositorio.ufpb.br

Barnes, R.; Lehman, C.; Mulla, D., 2014. An efficient assignment of drainage direction over flat surfaces in raster digital elevation models. Computers & Geosciences, v. 62, 128-135. http://dx.doi.org/10.1016/j.cageo.2013.01.009.

Benini, R.M.; Mendiondo, E.M., 2015. Urbanização e Impactos no Ciclo Hidrológico na Bacia do Mineirinho. Floresta e Ambiente, v. 22, (2), 211-222. https://doi.org/10.1590/2179-8087.103114.

Bork, C.; Castro, A.; Leandro, D.; Corrêa, L.; Siqueira, T., 2017. Índices de precipitação extrema para os períodos atual (1961-1990) e futuro (2011-2100) na bacia do rio Taquari-Antas, RS. Brazilian Journal of Environmental Sciences (Online), (46), 29-45. https://doi.org/10.5327/Z2176-947820170233.

Bravo, J.M.; Allasia, D.; Paz, A.R.; Collischonn, W.; Tucci, C.E.M., 2012. Coupled Hydrologic-Hydraulic Modelling of the Upper Paraguay River Basin. Journal of Hydrologic Engineering, v. 17, (5), 635-646. https://doi.org/10.1061/(ASCE)HE.1943-5584.0000494.

Buarque, D.C.; Fan, F.M.; Paz, A.R.; Collischonn, W., 2009. Comparação de Métodos para Definir Direções de Escoamento a partir de Modelos Digitais de Elevação. Revista Brasileira de Recursos Hídricos, v. 14, (2), 91-103. https://doi.org/10.21168/rbrh.v14n2.p91-103.

Caldas, A.M.; Pissarra, T.C.T.; Costa, R.C.A.; Rolim Neto, F.C.; Zanata, M.; Parahyba, R.D.B.V.; Fernandes, L.F.S.; Pacheco, F.A.L., 2018. Flood vulnerability, environmental land use conflicts, and conservation of soil and water: A study in the Batatais SP municipality, Brazil. Water, v. 10, (10), 1357. https://doi.org/10.3390/w10101357.

Centro de Estudos e Pesquisas em Engenharia e Defesa Civil/Universidade Federal de Santa Catarina (CEPED/UFSC), 2013. Atlas brasileiro de desastres naturais: 1991 a 2012. 2. ed. Centro Universitário de Estudos e Pesquisas sobre Desastres, Florianópolis. Available from: https://www.ceped.ufsc.br. Access on June 20, 2020.

Cirilo, J.A.; Alves, F.H.B.; Silva, L.A.C.; Campos, J.H.A.L., 2014. Suporte de informações georreferenciadas de alta resolução para implantação de infraestrutura e planejamento territorial. Revista Brasileira de Geografia Física, v. 7, (4), 755-763. https://doi.org/10.26848/rbgf.v7.4.p755-763.

Clement, M.; Kilsby, C.; Moore, P., 2018. Multi-temporal synthetic aperture radar flood mapping using change detection. Journal of Flood Risk Management, v. 11, (2), 152-168. https://doi.org/10.1111/jfr3.12303.

Cuartas, L.A.; Tomasella, J.; Nobre, A.D.; Nobre, C.A.; Hodnett, M.G.; Waterloo, M.J.; Oliveira, S.M.; Von Randow, R.C.; Trancoso, R.; Ferreira, M., 2012. Distributed hydrological modeling of a micro-scale rainforest watershed in Amazonia: Model evaluation and advances in calibration using the new

HAND terrain model. Journal of Hydrology, v. 462-463, 15-27. https://doi.org/10.1016/j.jhydrol.2011.12.047.

Degiorgis, M.; Gnecco, G.; Gorni, S.; Roth, G.; Sanguineti, M.; Taramasso, A.C., 2012. Classifiers for the detection of flood-prone areas using remote sensed elevation data. Journal of Hydrology, v. 470-471, 302-315. https://doi.org/10.1016/j.jhydrol.2012.09.006.

Fan, M.F.; Collischonn, W.; Sorribas, M.V.; Pontes, P.R.M., 2013. Sobre o início da rede de drenagem definida a partir dos modelos digitais de elevação. Revista Brasileira de Recursos Hídricos, v. 18, (3), 241-257. https://doi.org/10.21168/rbrh.v18n3.p241-257.

Farr, T.G.; Rosen, P.A.; Caro, E; Crippen, R.; Duren, R.; Hensley, S.; Kobrick, M.; Paller, M.; Rodriguez, E.; Roth, L.; Seal, D.; Shaffer, S.; Shimada, J.; Umland, J.; Werner, M.; Oskin, M.; Burbank, D.; Alsdorf, D., 2007. The Shuttle Radar Topography Mission. Reviews of Geophysics, v. 45, (2). https://doi.org/10.1029/2005RG000183.

Fernandes, R.; Valverde, M., 2017. Análise da resiliência aos extremos climáticos de chuva: estudo preliminar na região de Mauá no ABC Paulista – São Paulo. Brazilian Journal of Environmental Sciences (Online), (44), 1-17. https://doi.org/10.5327/Z2176-947820170183.

Folha de S.Paulo, 2004. Barragem rompe e inunda cidades da PB - Em Alagoa Grande e Mulungu ao menos três pessoas morreram e outras 1.600 estão desabrigadas, segundo a Defesa Civil. Available from: https://www1.folha.uol.com.br/fsp/cotidian/ff1906200430.htm. Access on June 20, 2020.

Garousi-Nejad, I.; Tarboton, D.G.; Aboutalebi, M.; Torres-Rua, A.F., 2019. Terrain Analysis Enhancements to the Height Above Nearest Drainage Flood Inundation Mapping Method. Water Resources Research, v. 55, (10), 7983-8009. http://dx.doi.org/10.1029/2019WR024837.

Gharari, S.; Hrachowitz, M.; Fenicia, F.; Savenije, H.H.G., 2011. Hydrological landscape classification: investigating the performance of HAND based landscape classifications in a central European meso-scale catchment. Hydrology and Earth System Sciences, v. 15, (11), 3275-3291. https://doi.org/10.5194/hess-15-3275-2011.

Goerl, R.F.; Michel, G.P.; Kobiyama, M., 2017. Mapeamento de áreas susceptíveis a inundação com o modelo HAND e análise do seu desempenho em diferentes resoluções espaciais. Revista Brasileira de Cartografia, v. 69, (1), 61-69. Available from: http://www.seer.ufu.br/index.php/revistabrasileiracartografia/article/view/44032. Access on April 11, 2020.

Governo do Estado da Paraíba. Agência Executiva de Gestão das Águas do Estado da Paraíba (AESA), 2006. Plano Estadual de Recursos Hídricos – PERH. Available from: http://www.aesa.pb.gov.br/aesa-website/wp-content/uploads/2020/03/PERH-Resumo-Executivo.pdf. Access on June 20, 2020

Hawker, L.; Bates, P.; Neal, J.; Rougier, J., 2018. Perspectives on Digital Elevation Model (DEM) simulation for flood modeling in the absence of a high-accuracy open access global DEM. Frontiers in Earth Science, v. 6, 1-9. https://doi.org/10.3389/feart.2018.00233.

Hdeib, R.; Abdallah, C.; Colin, F.; Brocca, L.; Moussa, R., 2018. Constraining coupled hydrological-hydraulic flood model by past storm events and post-event measurements in data-sparse regions. Journal of Hydrology, v. 565, 160-176. https://doi.org/10.1016/j.jhydrol.2018.08.008.

Heinzlef, C.; Becue, V.; Serre, D., 2020. A spatial decision support system for enhancing resilience to floods: bridging resilience modelling and geovisualization techniques. Natural Hazards and Earth System Sciences, v. 20, (4), 1049-1068. https://doi.org/10.5194/nhess-20-1049-2020.

Jenson, S.; Domingue, J., 1988. Extracting topographic sctruture from digital elevation data for Geographic Information System analysis. Photogrammetric

Engineering and Remote Sensing, v. 54, (11), 1593-1600. Available from: https://pubs.er.usgs.gov/publication/70142175. Access on August 16, 2020.

Jones, R., 2002. Algorithms for using a DEM for mapping catchment areas of stream sediment samples. Computers and Geosciences, v. 28, (9), 1051-1060. https://doi.org/10.1016/S0098-3004(02)00022-5.

Krieger, G.; Moreira, A.; Fiedler, H.; Hajnsek, I.; Werner, M.; Younis, M., Zink, M., 2007. TANDEM-X: A satellite formation for high-resolution SAR interferometry. IEEE Transactions on Geoscience and Remote Sensing, v. 45, (11), 3317-3341. https://doi.org/10.1109/TGRS.2007.900693.

Landuyt, L.; Van Wesemael, A.; Schumann, G.J.; Hostache, R.; Verhoest, N.E.C.; Van Coillie, F.M.B., 2019. Flood Mapping Based on Synthetic Aperture Radar: An Assessment of Established Approaches. IEEE Transactions on Geoscience and Remote Sensing, v. 57, (2), 722-739. https://doi.org/10.1109/TGRS.2018.2860054.

Li, J.; Li, T.; Zhang, L.; Sivakumar, B.; Fu, X.; Huang, Y.; Bai, R., 2020. A D8-compatible high-efficient channel head recognition method. Environmental Modelling and Software, v. 125, 104624. https://doi.org/10.1016/j.envsoft.2020.104624.

Lin, Q.; Leandro, J.; Wu, W.; Bhola, P.; Disse, M., 2020. Prediction of maximum flood inundation extents with resilient backpropagation neural network: Case study of Kulmbach. Frontiers in Earth Science, v. 8, 1-8. https://doi.org/10.3389/feart.2020.00332.

Lindsay, J.B., 2016. The practice of DEM stream burning revisited. Earth Surface Processes and Landforms, v. 41, (5), 658-668. https://doi.org/10.1002/esp.3888.

Lira, F.; Cardoso, A., 2018. Estudo de tendência de vazões de rios das principais bacias hidrográficas brasileiras. Brazilian Journal of Environmental Sciences (Online), (48), 21-37. https://doi.org/10.5327/Z2176-947820180273.

Liu, Y.Y.; Maidment, D.R.; Tarboton, D.G.; Zheng, X.; Wang, S., 2018. A CyberGIS Integration and Computation Framework for High-Resolution Continental-Scale Flood Inundation Mapping. Journal of the American Water Resources Association, v. 54, (4), 770-784. https://doi.org/10.1111/1752-1688.12660.

Mark, D.M., 1984. Automated detection of drainage networks from digital elevation model. Cartographica, v. 21, (2-3), 168-178. https://doi.org/10.3138/10LM-4435-6310-251R.

Marques, A.L.; Silva, J.B.; Silva, D.G., 2015. Compartimentação geológico-geomorfológica da bacia hidrográfica do rio Mamanguape-PB utilizando modelagem espacial. In: Anais XVII Simpósio Brasileiro de Sensoriamento Remoto, João Pessoa-PB, Brasil, 346-353. Available from: http://marte2.sid.inpe.br/rep/sid.inpe.br/marte2/2015/06.15.14.08.06. Access on August 16, 2020.

McGrath, H.; Bourgon, J.F.; Proulx-Bourque, J.S.; Nastev, M.; Abo El Ezz, A., 2018. A comparison of simplified conceptual models for rapid web-based flood inundation mapping. Natural Hazards, v. 93, 905-920. https://doi.org/10.1007/s11069-018-3331-y.

Mengue, V.P.; Scottá, F.C.; Silva, T.S.; Farina, F., 2016. Utilização do Modelo HAND para mapeamento das áreas mais suscetíveis à inundação no Rio Uruguai. Pesquisas em Geociências, v. 43, (1), 41-53. https://doi.org/10.22456/1807-9806.78191.

Meyer, V.; Becker, N.; Markantonis, W.; Schwarze, R.; van den Bergh, J. C. J. M.; Bouwer, L. M.; Bubeck, P.; Ciavola, P.; Genovese, E.; Green, C.; Hallegatte, S.; Kreibich, H.; Lequeux, Q.; Logar, I.; Papyrakis, E.; Pfurtscheller, C.; Poussin, J.; Przyluski, V.; Thieken, A. H.; Viavattene, C., 2013. Review article: Assessing the costs of natural hazards – state of the art and knowledge gaps. Natural

Hazards and Earth System Sciences, v. 13, (5), 1351-1373. https://doi.org/10.5194/nhess-13-1351-2013.

Momo, M.R.; Pinheiro, A.; Severo, D.L.; Cuartas, L.A.; Nobre, A.D., 2016. Desempenho do modelo HAND no mapeamento de áreas suscetíveis à inundação usando dados de alta resolução espacial. Revista Brasileira de Recursos Hídricos, v. 21, (1), 200-208. http://dx.doi.org/10.21168/rbrh.v21n1.p200-208.

Morelli, S.; Battistini, A.; Catani, F., 2014. Rapid assessment of flood susceptibility in urbanized rivers using digital terrain data: Application to the Arno river case study (Firenze, northern Italy). Applied Geography, v. 54, 35-53. http://dx.doi.org/10.1016/j.apgeog.2014.06.032.

Niipele, J.N.; Chen, J., 2019. The usefulness of Alos-Palsar DEM data for drainage extraction in semi-arid environments in The Iishana sub-basin. Journal of Hydrology: Regional Studies, v. 21, 57-67. https://doi.org/10.1016/j.ejrh.2018.11.003.

Nobre, A.D.; Cuartas, L.A.; Hodnett, M.; Rennó, C.D.; Rodrigues, G.; Silveira, A.; Saleska, S., 2011. Height Above the Nearest Drainage–a hydrologically relevant new terrain model. Journal of Hydrology, v. 404, (1-2), 13-29. https://doi.org/10.1016/j.jhydrol.2011.03.051.

Nobre, A.D.; Cuartas, L.A.; Momo, M.R.; Severo, D.L.; Pinheiro, A.; Nobre, C.A., 2016. HAND contour: a new proxy predictor of inundation extent. Hydrological Processes, v. 30, (2), 320-333. https://doi.org/10.1002/hyp.10581.

O'Loughlin, F.E.; Paiva, R.C.D.; Durand, M.; Alsdorf, D.E.; Bates, P.D., 2016. A multi-sensor approach towards a global vegetation corrected SRTM DEM product. Remote Sensing of Environment, v. 182, 49-59. https://doi.org/10.1016/j.rse.2016.04.018.

Paprotny, D.; Sebastian, A.; Morales-Nápoles, O.; Jonkman, S.N., 2018. Trends in flood losses in Europe over the past 150 years. Nature Communications, v. 9, 1985. https://doi.org/10.1038/s41467-018-04253-1.

Paul, G.C.; Saha, S.; Hembram, T.K., 2019. Application of the GIS-Based Probabilistic Models for mapping the flood susceptibility in Bansloi sub-basin of Ganga-Bhagirathi River and their comparison. Remote Sensing in Earth Systems Sciences, v. 2, 120-146. https://doi.org/10.1007/s41976-019-00018-6.

Paz, A.R.; Collischonn, W., 2008. Derivação de rede de drenagem a partir de dados do SRTM. Revista Geográfica Acadêmica, 2, (2), 84-95. Available from: https://go.gale.com/ps/i.do?id=GALE%7CA186470659&sid=-googleScholar&v=2.1&it=r&linkaccess=abs&issn=16787226&p=A-ONE&sw=w&userGroupName=anon%7E6ac0a33e. Access on July 20, 2020.

Paz, A.R.; Collischonn, W.; Tucci, C.E.M.; Padovani, C.R., 2011. Large-scale modelling of channel flow and floodplain inundation dynamics and its application to the Pantanal (Brazil). Hydrological Process, v. 25, (9), 1498-1516. https://doi.org/10.1002/hyp.7926.

Pontes, P.R.M.; Fan, F.M.; Fleischmann, A.S.; Paiva, R.C.D.; Buarque, D.C.; Siqueira, V.A.; Jardim, P.F.; Sorribas, M.V.; Collischonn, W., 2017. MGB-IPH model for hydrological and hydraulic simulation of large floodplain river systems coupled with open source GIS. Environmental Modelling & Software, v. 94, 1-20. https://doi.org/10.1016/j.envsoft.2017.03.029.

Prakash, M.; Cohen, R.; Hilton, J.; Khan, S.H., 2020. An evidence based approach to evaluating flood adaptation effectiveness including climate change considerations for coastal cities: City of Port Phillip, Victoria, Australia. Journal of Flood Risk Management, v. 13, (Suppl. 1), e12556. https://doi.org/10.1111/jfr3.12556.

Rahmati, O.; Kornejady, A.; Samadi, M.; Nobre, A.D.; Melesse, A.M., 2018. Development of an automated GIS tool for reproducing the HAND terrain model. Environmental Modeling & Software, v. 102, 1-12. https://doi.org/10.1016/j.envsoft.2018.01.004.

Rennó, C.D.; Nobre, A.D.; Cuartas, L.A.; Soares, J.V.; Hodnett, M.G.; Tomasella, J.; Waterloo, M.J., 2008. HAND, a new terrain descriptor using SRTM-DEM: Mapping terra-firme rainforest environments in Amazonia. Remote Sensing of Environment, v. 112, (9), 3469-3481. https://doi.org/10.1016/j.rse.2008.03.018.

Robinson, N.; Regetz, J.; Guralnick, R.P., 2014. EarthEnv-DEM90: A nearly-global, void-free, multi-scale smoothed, 90m digital elevation model from fused ASTER and SRTM data. ISPRS Journal of Photogrammetry and Remote Sensing, v. 87, 57-67. https://doi.org/10.1016/j.isprsjprs.2013.11.002.

Rodda, H.J.E., 2005. The Development and Application of a Flood Risk Model for the Czech Republic. Natural Hazards, v. 36, 207-220. https://doi.org/10.1007/s11069-004-4549-4.

Rodrigues, I.A.; Antunes, L.R.; Rodovalho, R.B., 2005. Perfis Social, Econômico e Ecológico da Área de Influência da APA da Barra do Rio Mamanguape (PB) - Bases para a classificação e seleção de estabelecimentos rurais para Gestão Ambiental. In: Rodrigues, G.S.; Buschinelli, C.C.A.; Rodrigues, I.A.; Neves, M.C.M. (Eds.), Avaliação de Impactos Ambientais para Gestão da APA da Barra do Rio Mamanguape/PB. EMBRAPA, São Paulo, pp. 40.

Santos, E.C.A.; Araújo, L.E.; Marcelino, A.S., 2015. Análise climática da Bacia Hidrográfica do Rio Mamanguape. Revista Brasileira de Engenharia Agrícola e Ambiental, v. 19, (1). http://dx.doi.org/10.1590/1807-1929/agriambi.v19n1p9-14.

Sedgewick, R. (1992). Algorithms in C++. Addison-Wesley, Reading.

Siqueira, V.A.; Fleischmann, A.; Jardim, P.F.; Fan, F.M.; Collischonn, W., 2016. IPH-Hydro Tools: a GIS coupled tool for watershed topology acquisition in an opensource environment. Revista Brasileira de Recursos Hídricos, v. 21, (1), 274-287. http://dx.doi.org/10.21168/rbrh.v21n1.p274-287.

Speckhann, G.A.; Chaffe, P.L.B.; Goerl, R.F.; Abreu, J.J.; Flores, J.A.A., 2018. Flood hazard mapping in Southern Brazil: a combination of flow frequency analysis and the HAND model. Hydrological Sciences Journal, v. 63, (1), 87-100. https://doi.org/10.1080/02626667.2017.1409896.

Tadono, T.; Takaku, J.; Tsutsui, K.; Oda, F.; Nagai, H., 2015. Status of "ALOS World 3D (AW3D)" global DSM generation. IEEE International Geoscience and Remote Sensing Symposium (IGARSS), Milão, 3822-3825. https://doi.org/10.1109/IGARSS.2015.7326657.

Tehrany, M.S.; Pradhan, B.; Mansor, S.; Ahmad, N., 2015. Flood susceptibility assessment using GIS-based support vector machine model with different kernel types. Catena, v. 125, 91-101. http://dx.doi.org/10.1016/j.catena.2014.10.017.

Van Zyl, J.J., 2001. The Shuttle Radar Topography Mission (SRTM): a breakthrough in remote sensing of topography. Acta Astronautica, v. 48, (5-12), 559-565. https://doi.org/10.1016/S0094-5765(01)00020-0.

Wu, T.; Li, J.; Li, T.; Sivakumar, B.; Zhang, G.; Wang, G., 2019. High-efficient extraction of drainage networks from digital elevation models constrained by enhanced flow enforcement from known river maps. Gemorphology, v. 340, 184-201. https://doi.org/10.1016/j.geomorph.2019.04.022.

Yamazaki, D.; Ikeshima, D.; Tawatari, R.; Yamaguchi, T.; O'Loughlin, F.; Neal, J.C.; Sampson, C.C.; Kanae, S.; Bates, P.D., 2017. A high-accuracy

map of global terrain elevations. Geophysical Research Letters, v. 44, (11), 5844-5853. https://doi.org/10.1002/2017GL072874.

Zambrano, F.C.; Kobiyama, M.; Pereira, M.A.F.; Michel, G.P.; Fan, F.M., 2020. Influence of different sources of topographic data on flood mapping: urban area São Vendelino municipality, southern Brazil. Revista Brasileira de Recursos Hídricos, v. 25, e40. https://doi.org/10.1590/2318-0331.252020190108.

Zheng, X.; Maidment, D.R.; Tarboton, D.G.; Liu, Y.Y.; Passalacqua, P., 2018a. GeoFlood: Large-scale flood inundation mapping based on high-resolution terrain analysis. Water Resources Research, v. 54, (12), 10013-10033. https://doi.org/10.1029/2018WR023457.

Zheng, X.; Tarboton, D.G.; Maidment, D.R.; Liu, Y.Y.; Passalacqua, P., 2018b. River Channel Geometry and Rating Curve Estimation Using Height above the Nearest Drainage. Journal of the American Water Resources Association, v. 54, (4), 785-806. https://doi.org/10.1111/1752-1688.12661.